

Table DR1. Major, trace and Sr-isotope compositions of El Barronal hyaloclastites and lavas

Group	<i>El Monsul</i>	<i>El Monsul</i>	<i>El Monsul</i>
Formation	El Barronal	El Barronal	El Barronal
Locality:	<i>Calas del Barronal</i>	<i>Calas del Barronal</i>	<i>Calas del Barronal</i>
Latitude:	36°43'59"N	36°43'56"N	36°43'56"N
Longitude:	02°07'34"W	02°07'34"W	02°07'34"W
Sample:	ALM 15	ALM 16	ALM 56
Type of Rock:	<i>columnar lava</i>	<i>glassy hyaloclast</i>	<i>glassy matrix</i>
Lithology:	<i>hK-dacite</i>	<i>hK-dacite</i>	<i>hK-dacite</i>
SiO₂ wt.%	62.1	60.5	59.4
TiO₂	0.56	0.52	0.57
Al₂O₃	16.6	15.3	14.1
Fe₂O₃	1.12	2.28	2.27
FeO	3.68	2.79	2.89
MnO	0.08	0.09	0.08
MgO	2.98	3.26	3.85
CaO	5.68	5.68	5.42
Na₂O	3.11	2.99	3.23
K₂O	2.38	2.24	1.76
P₂O₅	0.13	0.09	0.10
LOI	1.57	4.20	6.32
Mg #	57.1	58.5	62.1
Sc ppm	19	19	18
V	132	120	127
Cr	25	28	30
Co	11	11	10
Ni	6	5	8
Cu	29	28	30
Zn	51	44	50
Ga	19	18	19
Rb	110	93	101
Sr	233	231	248
Y	15.8	16.2	15.2
Zr	118	121	119
Nb	4.3	4.3	4.7
Cs	10.6	11.7	8.9
Ba	243	263	213
⁸⁷Sr/⁸⁶Sr_m	0.713792	0.713789	0.713845
2σ	0.000006	0.000007	0.000007
⁸⁷Sr/⁸⁶Sr_i	0.713550	0.713580	0.713633

Major (wt%) and trace (ppm) elements have been performed by XRF (X-ray fluorescence), whereas Sr-isotope using Thermal Ionization Mass Spectrometry (TIMS) after Sr purification and separation. Leaching prior to sample digestion has been performed prior to isotopic determination.

$$\text{Mg \#} = 100 * [\text{Mg}/(\text{Fe}+\text{Mg})]$$

$^{87}\text{Sr}/^{86}\text{Sr}_m$ are the measured isotopic compositions with 2σ being the internal error, and $^{87}\text{Sr}/^{86}\text{Sr}_i$ are the initial, age-corrected, values.

Note that sample ALM 15 is representative of the lava flow interior, whilst samples ALM 16 and ALM 56 are from the hyaloclastite carapace representing glassy hyaloclast and the glassy matrix, respectively.

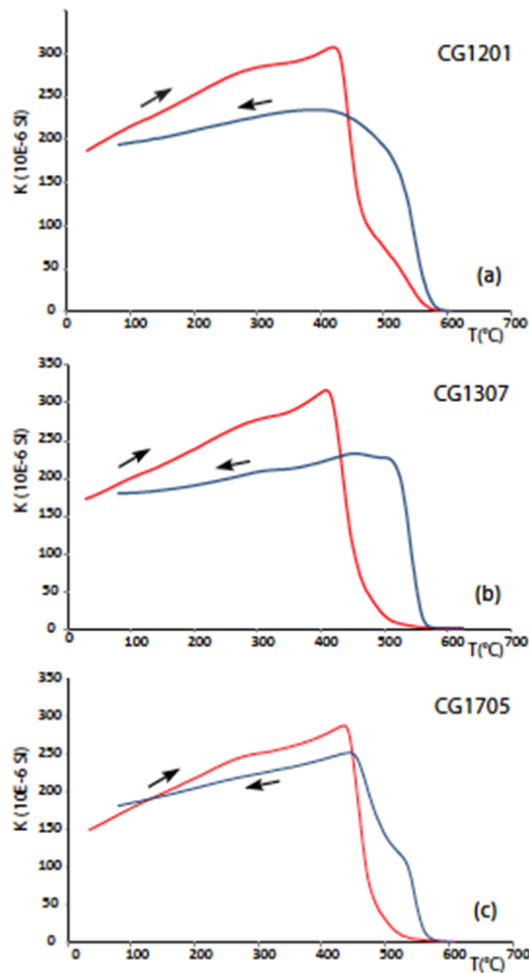
Note that initial isotopic Sr does not change in the three different fractions of the magmatic body, whereas the LOI, and then the major oxides, vary largely from the lowest LOI value in the fresh lava, possibly close to the original volatile content of the lava, to the highest LOI values of the glassy hyaloclast and the glassy matrix, which have acquired secondary water during glass palagonitisation.

Age interval of El Barronal coherent lava is 12.19-12.67 Ma. See Soriano et al. (2013) for further details.

Methods

Samples from coherent lava were sampled by drilling machine and oriented using a standard procedure; whereas the samples from hyaloclastite were collected by hand following the procedure of Cioni et al. (2004). The remanent magnetization was measured by a JR6A spinner magnetometer (Measuring range from 0 to 12500 A/m; Noise 2.4 μ A/m). Samples were thermally demagnetized from ambient to Curie temperature during progressive steps (9–13), with temperature intervals of 30–50°C. Results were analyzed by principal component analysis (Kirschvink, 1980) in order to determine sample characteristic remanent magnetization (ChRM) directions. The paleomagnetic mean directions were computed by Fisher (1953) statistics. 12 samples from coherent lava and 10 from hyaloclastite, characterized by unstable paleomagnetic behavior (i.e. MAD>15°), were rejected for further analyses. Principal component analyses and Fisher statistic were computed using Remasoft3.0 software (Chadima and Hrouda, 2006). In order to define the Curie temperature of the magnetic minerals and to exclude the presence of any thermal mineralogical alteration during the heating process, magnetic susceptibility was measured as a function of temperature in air, from room temperature to 700°C for representative samples selected from the coherent lava and hyaloclastite facies. We used a AGICO CS3 furnace in connection with KLY-3S (Sensitivity to susceptibility changes: 1 x 10E-7 SI; Temperature range: ambient temperature to 700°C). All the magnetic, paleomagnetic and rock magnetic measurements were performed at the Paleomagnetic Laboratory of the University of Roma Tre.

Figure DR1. Thermomagnetic curves of El Barronal lava and hyaloclastite samples.



Magnetic susceptibility versus temperature curves from coherent lava (a) and from sub-vertical (b) and shallowly-dipping (c) hyaloclastite samples. The heating curves (in red) show a similar trend indicating similar magnetic mineral content. In particular, the three different curves suggest the presence of low-Ti titano-magnetite and stoichiometric magnetite, as showed by the steep decays in magnetic susceptibility curves, resulting in Curie temperatures of 450°C and 580°C respectively.

Table DR2. Paleomagnetic directions and blocking temperatures for each NRM component of the dike samples

Sample	Comp.	D	I	MAD	Tub
CG0101	SC	294.7	38.4	2.2	520
CG0102	SC	285.6	48.7	0.9	520
CG0103	SC	279.4	50.4	1.1	520
CG0117	SC	299.6	61.1	4.1	520
CG0119	SC	343.3	60.3	3	520
CG0120	SC	7.2	49.2	3	520
CG0121	SC	323.5	51.3	9.5	520
CG0201	SC	332.2	57.7	3.5	560
CG0202	SC	324.5	56.1	3	560
CG0203A	SC	324.9	52.9	12.6	380
CG0207	SC	356.6	74.7	7.1	610
CG0208	SC	339.5	59	4.4	630
CG0209	SC	351.5	47.4	5.4	380
CG0210	SC	354.8	64.4	12.7	280
CG0210B	SC	343	75.5	3.1	320
CG0211	SC	343.1	60	6.9	480
CG1101A	SC	360	47.4	4.7	580
CG1102B	SC	14.8	53.4	6.8	580
CG1103	SC	330.9	53.5	5.7	540
CG1107A	SC	9.5	70	8.2	580
CG1118	SC	350.1	76.1	7.4	480
CG1120	SC	343.2	67.2	11.4	580
CG1203A	SC	55	55.5	2.3	630
CG1204B	SC	7.6	56.2	2.2	580
CG1205	SC	10.1	59.9	3.8	580
CG1206	SC	8.1	59	3.6	560
CG1207	SC	5.2	56.5	4.9	560
CG1212	SC	359.5	58.2	1.8	580
CG1213A	SC	359.8	56.5	3.6	580
CG1216B	SC	326.9	63.5	1.3	520
CG1222	SC	359.3	54.5	2.1	480
CG1224	SC	358.3	58.7	3.4	520
CG1225	SC	2.8	54.5	2.3	520
CG1228	SC	0.5	56.9	1.2	580

Paleomagnetic directions and temperature values for each component of the subvertical hyaloclasite samples.

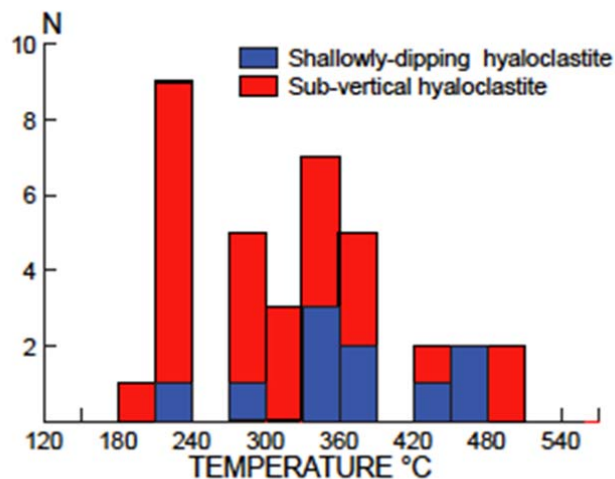
Sample	Comp.	D	I	MAD	DT/Tub		Comp.	D	I	MAD	DT
CG0601	LT	346.4	43.5	4.6	20-280		HT	8.5	24.8	17.3	350-580
CG0602	LT	355.5	42.9	12.3	20-280		HT	16	23.7	11	350-630
CG0603	LT	358.5	41.4	4.6	20-180		HT	296.4	-23.4	8.6	220-630
CG0604	LT	9.9	54.9	12.4	20-280		HT	45.9	14.8	6.8	350-630
CG0605	LT	313.2	51.1	4.8	20-480		HT	15.8	48.5	14.8	480-580
CG0606	LT	321.8	77.6	10	20-350		HT	19	49	6.4	420-630
CG0607	LT	337	50.7	13.9	20-220		HT	94.6	-47.3	19	220-630
CG0608	LT	22.8	40.9	3.9	20-220		HT	241	-16.2	15	220-580
CG0609	LT	0.9	44.5	4.6	20-280		HT	7	18.1	11.2	280-580
CG0701	LT	21.4	52.7	14	20-220		HT	97	43.7	12	280-580
CG0702	LT	319.9	29.2	9	100-220		HT	5.7	33.1	9.2	280-630
CG0703	SC	338.5	55.6	13.2	580		-	-	-	-	-
CG0704	LT	355.5	55.3	10.4	20-220		HT	314	44.7	15	280-580
CG0705	SC	347.1	60.9	12.3	630		-	-	-	-	-
CG0706	LT	3.7	50.7	13	20-280		HT	290.6	31.5	4.5	320-580
CG0707	LT	49.4	46	11.6	20-220		HT	318.7	52.9	8.9	280-580
CG0708	LT	328.3	47.4	12.3	20-280		HT	30.8	65.4	7.8	320-630
CG13B01	LT	272.5	59.1	5.4	20-200		HT	272.5	59.1	5.4	220-580
CG13B02	LT	351.2	81.2	8.6	20-420		HT	324.1	10.3	8.5	460-600
CG13B03	LT	349.6	48.8	6.3	20-340		HT	317.9	-30.8	11.6	380-520
CG13B04	LT	158.8	51.3	7.7	20-300		HT	355.3	49.1	9.4	340-560
CG13B05	SC	58.2	51	7.5	340		-	-	-	-	-
CG13B06	SC	256.1	81.8	10.5	460		-	-	-	-	-
CG13B07	LT	230.6	47.4	13.2	20-300		HT	66.3	41.9	18.6	320-560
CG13B08	LT	76.6	60.6	13.7	100-340		HT	14.3	25.2	10.1	380-560
CG1401	SC	57.8	49.9	9.8	580		-	-	-	-	-
CG1402	SC	338.6	54.3	10.9	20-320		-	-	-	-	-
CG1403	SC	30.6	81.7	7.9	20-580		-	-	-	-	-
CG1404	SC	6.5	60.1	4.1	120-580		-	-	-	-	-
CG1405	SC	345	32.6	1.4	20-440		-	-	-	-	-
CG1406	SC	75.7	67.4	10.1	20-630		-	-	-	-	-
CG1407	LT	354.9	23	7.5	20-320		HT	354.9	23.1	7.5	230-610
CG1408	SC	45.2	24	9.9	20-510		-	-	-	-	-
CG1409	SC	328.6	23.6	11.5	20-440		-	-	-	-	-
CG1410	LT	263.1	78.8	9.4	20-480		HT	40	7.9	6.7	510-610
CG1411	SC	250.5	69.2	6.8	140-540		-	-	-	-	-
CG1412	SC	331.4	25.7	6.4	140-580		-	-	-	-	-
CG1413	SC	330	33.8	9.4	180-580		-	-	-	-	-
CG1414	LT	1.3	33.1	8.6	20-320		HT	278.1	14.9	8.2	380-580
CG1416	SC	7.6	8.2	8.9	540		-	-	-	-	-
CG1417	SC	321.4	44.8	7.2	510		-	-	-	-	-
CG1418	LT	33.4	62.8	10.2	20-380		HT	284.4	36.2	14.4	420-540
CG1420	SC	341.1	42	5.9	580		-	-	-	-	-

Paleomagnetic directions and temperature values for each component of the shallowly-dipping hyaloclastite samples

Sample	Comp.	D	I	MAD	DT/Tub		Comp.	D	I	MAD	DT
CG1501	LT	13.4	69.3	13.6	100-300		HT	307.6	36.5	13.2	340-540
CG1502	SC	10.9	41.7	8.3	100-580		-	-	-	-	-
CG1503	SC	253.1	14.4	2.4	420		-	-	-	-	-
CG1504	LT	221.1	59.2	14.1	100-340		HT	24.8	26.9	10	400-580
CG1505	SC	350.4	48.9	12	460		-	-	-	-	-
CG1506	LT	7.3	32.3	6.2	150-460		HT	41.8	-5.6	12.1	500-600
CG1702	SC	305.4	39.9	8.8	560		-	-	-	-	-
CG1703	LT	2.5	30.7	10.2	150-420		HT	294.8	-2.6	7	460-560
CG1705	LT	3	69	6.7	20-340		HT	31.4	41.3	14.1	380-560
CG1707	LT	11	43.6	11.2	150-460		HT	256.2	36.4	8.2	500-600
CG1708	SC	331.6	36.6	6.2	520		-	-	-	-	-
CG1709	SC	57.7	32.1	11.4	560		-	-	-	-	-
CG1710	SC	313	53.3	12.2	600		-	-	-	-	-
CG1801	SC	272.3	41.3	8.7	560		-	-	-	-	-
CG1802	SC	299.6	52.7	9.1	580		-	-	-	-	-
CG1804	SC	347.1	32.5	10.7	460		-	-	-	-	-
CG1806	LT	135	70.5	6.3	100-380		HT	312.9	48.8	13.3	420-560
CG1807	LT	293	-24.3	9.9	100-380		HT	298.6	61.3	11.6	420-600
CG1808	LT	26	29.3	17.5	100-340		HT	307.7	37.3	9.4	380-560
CG1809	SC	358.9	37.9	12.6	580		-	-	-	-	-
CG1810	SC	321.6	43.1	11.1	520		-	-	-	-	-

Sample ID: sample name. Component: single component (SC); in the case of two components of magnetization, we distinguish low-temperature (LT) and high-temperature (HT) component. D, I: paleomagnetic declination and inclination in degrees. MAD: maximum angular deviation calculated for each component. Tub: estimated blocking temperature for single component (Celsius degree). DT: temperature interval (lowest and highest temperatures) for LT and HT components (Celsius degree).

Figure DR2. Frequency histogram of emplacement temperature estimations.



Emplacement temperature estimations for sub-vertical (red columns) and shallowly-dipping (blue columns) hyaloclastites according to paleomagnetic data. Most of the analyzed samples show unblocking temperatures for low-temperature component between 210°C and 390°C.

Calculations

Simple cooling models can be used to evaluate the rapid cooling rates expected for a submarine magma in contact with cold seawater. Considering a model of conductive heat flow in two linear half spaces (Carslaw and Jaeger, 1959), for an initial $T = 1050$ °C and thermal diffusivity of 10×10^{-6} m² s⁻¹, calculation can be made for the evolution of temperature and cooling rates (Wilding et al., 2000). Farther from the interface, where instantaneous cooling rates up to 4320 K /min can be expected (Nichols et al., 2009), cooling rates of 35 to 10 K/min are calculated, values which agree very well with measured cooling rates for hyaloclastite samples via heat capacity measurements by Wilding et al. (2000). We calculated the effect of cooling rate on the viscosity of the magma at Tg via the following empirical equation (Scherer 1986; Stevenson et al., 1995; Gottsmann et al., 2002):

$$\log \eta^* = K - \log_{10} |q| \quad (1)$$

There η^* is the viscosity at Tg, K is termed the shift factor, and q is the cooling rate, expressed as K/s. The absolute value of K can be approximated to a composition-dependent term, described by Gottsmann et al. (2002) as:

$$K = 10.321 - 0.175 * \ln X \quad (2)$$

where X is the molar percentage of excess (network modifying) oxides (Potuzak et al., 2008). Eq. (2) yields a shift factor for the present composition of 9.99 for H₂O = 0.05 wt% and 9.87 for H₂O = 2.00 wt%. Once that viscosity at Tg is known, Tg can be easily calculated for the composition of interest following Giordano et al. (2008) model.

REFERENCES CITED IN DATA REPOSITORY

- Carslaw, H.S., and Jaeger J.C., 1959, Conduction of heat in solids. 2nd Edition. Clarendon, Oxford.
- Chadima, M., and Hrouda, F., 2006, REMASOFT 3.0 a user-friendly paleomagnetic data browser and analyzer: *Travaux Géophysiques*, v. 27, p. 20–21.
- Cioni, R., Gurioli, L., Lanza, R., and Zanella E., 2004, Temperature of the A.D. 79 pyroclastic density current deposits (Vesuvius, Italy): *Journal of Geophysical Research*, v. 109, B02207, doi:10.1029/2002JB002251.
- Fisher, R.A., 1953. Dispersion on a sphere: *Proceedings of the Royal Society of London, Series A*, 217, 295–305.
- Giordano, D., James, K. Russell, J.K., and Dingwell, D.B., 2008, Viscosity of magmatic liquids: A model: *Earth and Planetary Science Letters*, v. 271, p. 123–134, doi:10.1016/j.epsl.2008.03.038.
- Gottsmann, J., Giordano, D., and Dingwell, D.B., 2002, Predicting shear viscosity during volcanic processes at the glass transition: a calorimetric calibration: *Earth and Planetary Science Letters*, v. 198, p. 417–427, doi:10.1016/S0012-821X(02)00522-8.
- Kirschvink, J.L., 1980, The least-squares line and plane and the analysis of palaeomagnetic data: *Geophysical Journal Royal Astronomical Society*, v. 62, p. 699–718.
- Nichols, A.R.L., Potuzak, M. and Dingwell, D.B., 2009. Cooling rates of basaltic hyaloclastites and pillow lava glasses from the HSDP2 drill core. *Geochimica et Cosmochimica Acta*, 73(4): 1052–1066.
- Potuzak, M., Nichols, A.R.L., Dingwell, D.B., and Clague, D.A., 2008, Hyperquenched volcanic glass from Loihi Seamount, Hawaii: *Earth and Planetary Science Letters*, 270, 54–62, doi:10.1016/j.epsl.2008.03.018.
- Scherer, G.W., 1986, Relaxation in glass and composites. Wiley, New York, pp 1–331.
- Soriano, C., Giordano, G., Cas, R., Riggs, N., and Porreca, M. (2013). Facies architecture, emplacement mechanisms and eruption style of the submarine andesite El Barronal complex, Cabo de Gata, SE Spain: *Journal of Volcanology and Geothermal Research*. doi:10.1016/j.jvolgeores.2013.07.001.
- Stevenson, R.J., Dingwell, D.B., Webb, S.L., and Bagdassarov, N.S., 1995, The equivalence of enthalpy and shear stress relaxation in rhyolitic obsidians and quantification of the liquid–glass transition in volcanic processes: *Journal of Volcanology and Geothermal Research*, v. 68, p. 297–306, doi.org/10.1016/0377-0273(95)00015-1.
- Wilding, M., Dingwell, D.B., Batiza, R., and Wilson, L., 2000, Cooling rates of hyaloclastites: applications of relaxation geospeedometry to undersea volcanic deposits: *Bulletin of Volcanology*, v. 61, p. 527–536, doi:10.1007/s004450050003.